

**SYSTEMATIC DEVELOPMENT OF FRAMEWORK FOR VALIDATION
AND PERFORMANCE QUANTIFICATION OF ADDITIVELY
MANUFACTURED REPLACEMENT PARTS FOR STRUCTURAL STEEL
APPLICATIONS**

**Thomas G Gallmeyer^{1*}, Jinesh Dahal¹, Branden B Kappes^{1*}, Aaron P Stebner^{1*},
Ravi S Thyagarajan², Juan A Miranda³, Adam Pilchak⁴, Jacob Nuechterlein⁵**

¹Department of Mechanical Engineering, Colorado School of Mines, Golden, CO

*Alliance for the Development of Additive Processing Technologies (ADAPT)

²Directorate of Systems Integration S&T, US Army Futures Command, Austin, TX

³Army Field Support Battalion, Fort Carson, CO

⁴Air Force Research Laboratory, Wright-Patterson Air Force Base, OH

⁵Elementum 3D, Erie, CO

ABSTRACT

Timely part procurement is vital to the maintenance and performance of deployed military equipment. Yet, logistical hurdles can delay this process, which can compromise efficiency and mission success for the warfighter. Point-of-need part procurement through additive manufacturing (AM) is a means to circumvent these logistical challenges. An Integrated Computational Materials Engineering framework is presented as a means to validate and quantify the performance of AM replacement parts. Statistical modeling using a random forest network and finite element modeling were to inform the build design. Validation was performed by testing coupons extracted from each legacy replacement parts, as well as the new additively manufactured replacement parts through monotonic tensile and combined tension-torsion fatigue testing. Destructive full hinge assembly tests were also performed as part of the experimental characterization. Lastly, the collected experimental results were used to iterate on the part design to showcase the advantages AM offers for meeting new service requirements.

Citation: T.G. Gallmeyer, J. Dahal, B.B. Kappes, A.P. Stebner, R.S. Thyagarajan, J.A. Miranda, A. Pilchak, J. Nuechterlein, “Systematic Development of Framework for Validation and Performance Quantification of Additively Manufactured (AM) Replacement Parts for Structural Steel Applications”, In *Proceedings of the Ground Vehicle Systems Engineering and Technology Symposium (GVSETS)*, NDIA, Novi, MI, Aug. 13-15, 2019.

1. INTRODUCTION

Part procurement for deployed military equipment can be an arduous, time-consuming, and expensive process resulting from supply chain

issues as demand changes [1]. These bottlenecks in procurement can render critical pieces of equipment inoperable or unsafe for use by our service members for extended periods of time.

Thus, as a means to reduce this downtime, it is desirable to have the ability to produce temporary, reliable parts at point-of-need in theater while traditional replacements are sourced [2].

Additive manufacturing (AM) is one such technology capable of meeting this need, as parts of various geometries and sizes can be rapidly produced [3], allowing for redeployment in hours to days instead of weeks to months. While AM serves as an attractive option to address the issues associated with part procurement, qualifying the reliability of these AM parts still poses a challenge [4], [5].

The practical application of this research is to develop a method that can be used to quantify the ability of AM replacement parts to substitute for the original design. While it would be ideal if the AM part met or even exceeded the performance of the legacy part, in reality, simply knowing what percentage of the legacy part performance can be achieved by the AM part is extremely useful in determining how best to use it. This is what we mean by performance quantification and describes the uniqueness of this research approach. The goal is to be able to execute this accurately using minimal physical testing of specimens either cut out of the AM parts, or alternatively from specimens made specifically for this purpose (i.e. witness specimens) from the same build as the AM parts. The comparative performance of AM vs legacy parts, even when manufactured using the same machine with the same processing parameters and out of the same material, will differ from case to case, depending on the actual part and the loading scenario. It is therefore the overarching objective of this research to define a simple and general methodology that will reliably quantify the performance of the AM part.

Thus, we will present an Integrated Computational Materials Engineering (ICME) framework that consists of statistical modeling of pre-existing data, finite element modeling, and targeted, small numbers of experimental validation tests as a means to systematically validate AM steel

replacement parts and quantify their performance versus the production legacy part. Being able to produce AM parts at the point of need in theater, and adequately quantifying its performance is critical to empowering the warfighter and ensuring mission success. This project is designed to give the Army a continuously improving framework for designing and quantifying the performances of AM replacement parts.

2. Experimental

As the focus of this study, a currently cold-rolled and cast steel door hinge assembly of a MAXXPRO Mine-Resistant Ambush Protected (MRAP) vehicle was the selected part (Figure 1). To manufacture the AM replacement parts, 17-4 PH stainless steel was chosen—a martensitic steel with good corrosion resistance and hardness properties that can be precipitation hardened through post-processing heat treatment.



Figure 1. MAXXPRO MRAP showing location and CAD model of door hinge assembly.

2.1. Integrated Computational Materials Engineering (ICME) Framework

Data were collected for 241 samples across three materials systems—17-4 PH stainless steel, 316L stainless steel, and Ti-6Al-4V—printed on three

powder bed systems: EOS, Renishaw, and Arcam systems, respectively. Cylindrical samples were printed at 40 mm part spacing to span the build field (+X, measured from the center of the build plate in the direction of the recoater blade and +Y measured from the center of the build plate into machine) and at 10, 20, and 40 mm part spacings. Round tensile bar samples were machined from these cylindrical samples to measure tensile yield strength, ultimate tensile strength, elastic modulus, percent elongation, and area reduction.

A random forest network (RFN) is a type of ensemble algorithm, one that aggregates the results from weak learners (estimators) to develop a model more accurate than any of the individual estimators [6]. This RFN used 374 estimators. To mitigate overfitting, the estimators were restricted to a maximum depth of 30. Max polling and arithmetic mean were used for leaf node reduction for categorical and continuous-valued data, respectively. Model variance was estimated using the jackknife method [7]; out-of-sample error was estimated from 3-fold cross validation.

2.2. Finite Element Analysis

Finite Element Analysis (FEA) was performed using commercial software ABAQUS to determine the stresses in each component of the hinge and door assembly. All displacements and rotations on the holes in the hinge were fixed to replicate the hinge being bolted to the body of the vehicle. Self-weight of the door and an additional 1200 N (to simulate human interactions) were the loads acting on the entire assembly. In-built surface-to-surface contact algorithm was used for all the contact surfaces interactions with the finer meshed part always acting as the master surface. After mesh optimization with criteria of stress variation of 20 MPa, approximately 2 million 8-node quadratic tetrahedral elements (referred to as C3D8R in ABAQUS) were used for the simulation.

2.3. Sample Fabrication for Validation

Fabrication of AM replacement parts was performed in argon atmosphere using standard EOS 17-4 PH powders (gas-atomized in argon) on an EOS M-290 direct metal laser sintering (DMLS) printer. Proprietary, manufacture-provided process parameters were used for build productions. An example of one of the completed builds is shown in Figure 2(a).

Test specimens were then machined from both the legacy replacement parts, as well as their AM replicates, by electrical discharge machining (EDM) or lathe-machined.

Tension-torsion fatigue specimens were lathe-machined from the hinge pins (Figure 2(b),(d)), while monotonic tensile specimens were electrical discharge machined from the hinge plates (Figure 2(c),(e)). Both specimen geometries were pursuant of ASTM E8/E8M-16a (Figure 2(d)-(e)). For the monotonic tensile specimen, sample orientation was such that the gage length was parallel to (0°, LG1), diagonal to (45°, LG2), and perpendicular to (90°, LG3; SM) the build direction for the AM replacement part to examine possible anisotropy in mechanical responses (Figure 2(c)). For consistency, the same specimen orientations were machined from the legacy replacement part, as well.

Post-machining heat treatment was applied to a subset of each specimen geometry. Specimens were initially solution-annealed at 1040 °C for 30 min, water quenched, and then aged at 482 °C for 1 h and air-cooled, all performed in atmosphere. The surfaces of all specimens were unaltered from their final post-processing state (either as-machined or as-heat treated surface finish).

2.4. Mechanical Testing

Monotonic tensile testing of all examined conditions was performed on an MTS Bionix Servohydraulic Test System (model 370.02) equipped with an MTS 662.20H-05 load cell. A cross-head speed of 2.25 mm/min was used, corresponding to an approximate strain rate of

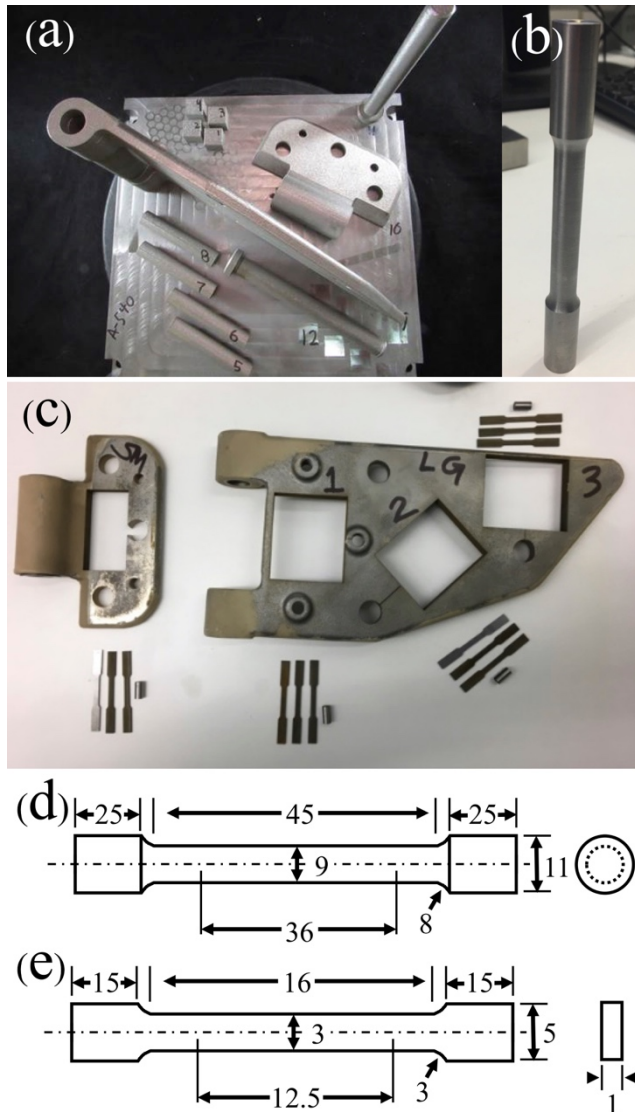


Figure 2. (a) Build plate of AM replacement parts. (b) Tension-torsion fatigue specimen machined from legacy and AM pins featured in (a). (c) Various orientations sampled from the hinge plates for monotonic tensile testing. (d-e) Specimen geometries used for tension-torsion fatigue (b) and monotonic tensile testing, respectively.

0.003 s^{-1} . Gage strains were calculated using a “virtual extensometer” from displacements measured using stereo digital image correlation (DIC). Images were acquired for stereo DIC using two FLIR GS3-U3-23S6M-C cameras orientated at an angle of 25° to the normal direction of the surface of the sample being tested. Schneider Unifoc-12 lenses (P/N 25-014780), each

configured with 60 mm of extension tubes, red (670 nm) bandpass filters to enhance black and white contrast, and linear polarizers to reduce glare, were set to a working distance of 290 cm to achieve a 30 x 22 mm field of view. Calibration was performed with a 6.38 x 6.38 mm Correlated Solutions optical measuring calibration target and the Correlated Solutions stereo DIC calibration routine. A high-intensity LED illuminator also fitted with a linear polarizer that was balanced to the lens polarizers was used to illuminate the samples. Strain computations were performed in Correlated Solutions VIC-3D 8. Facet size of 90 pixels and a step size of 40 pixels was used for all the strain computations to maintain consistency. Static and translated images were acquired to determine a noise value of 10^{-4} mm/mm in the calculated strains from stereo DIC.

Tension-torsion fatigue tests were conducted on the MTS Bionix Servohydraulic Test System used for monotonic failure. Specimens were tested at a static tensile stress of 280 MPa with fully alternating 280 MPa torque at 2 Hz. Runout criterion was set at 1 million fully-reversed cycles. This combined stress state was used to mimic the conditions calculated from FEA and will be discussed further in Section 3.

Full hinge-assembly failure by three-point bend testing was conducted on an MTS Landmark Servohydraulic Test System (model 370.25) equipped with an MTS 661.22H-01 load cell. A modified I-beam fixture was used secure each hinge assembly in place, and the load was applied to the pin of each assembly. A crosshead displacement speed of 4 mm/min was used for each test.

3. Results and Discussion

3.1. ICME Framework for Accelerated Part Qualification

The proposed framework for the accelerated part qualification process is schematically outlined in Figure 3. Detailed in the subsequent sections are the

efforts on how a preexisting database, coupled with data informatics, modeling, and advanced engineering tools, can be utilized to manufacture AM replacement parts and experimentally verify their performance.

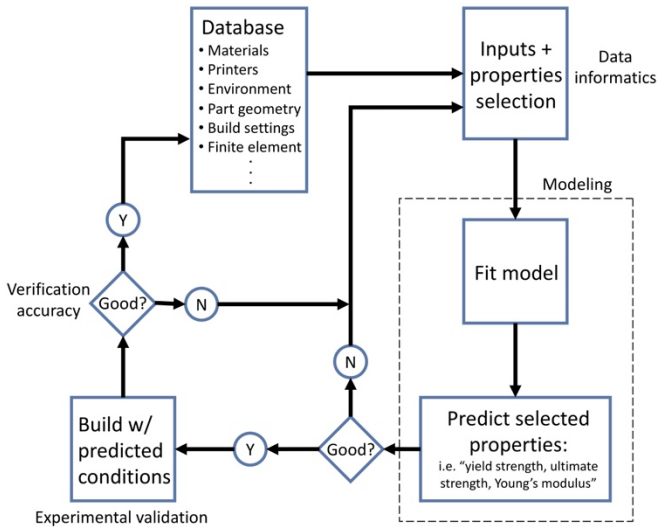


Figure 3. Schematic representation of the Integrated Computational Materials Engineering framework proposed in this paper.

Data Informatics and Modeling

The results of the model fit for all alloys across all build configurations are shown in Figure 4. When fit across multiple compositions alloy mechanical properties are, unsurprisingly, dominated by gross compositional differences. The intraclass variance is small in comparison to the compositional variance. The estimated model error across alloy systems is able to capture the variability in yield strength. The distribution in the model predicted error (orange histogram) from Figure 4(b), is tighter than an ideal normal distribution (blue line), indicating that the error estimate from cross validation and jackknifing overestimates the actual system error. The intraclass variance is captured for models trained exclusively on the data for each alloy subset. The predicted-versus-actual plot in Figure 4(c) presents the efficacy of this model in capturing the 5-7% variability in 17-4 PH yield strength. 74% of this variability is captured by part

spacing, and only approximately 20% based on the X-Y position of the part. A wider estimated error in the yield strength for 17-4 PH, see Figure 4(d), than ideal indicates that this model underestimates the actual error.

The predicted versus actual curve of Figure 4(a) presents a model fit across three compositions, forming three clusters that are, from bottom left to top right, SS 316L, 17-4 PH, and Ti-6Al-4V. The distribution of points in this plot reveals two things about the performance of this model: that the best predictors of yield strength of these materials are those features related to the composition and that the intraclass variation. The variation within the alloy is not captured in a model dominated by compositional features; the intrinsic and model errors are too large to simultaneously capture both the effect of composition and the effect of part geometry and process type. However, this is not the same as saying that no geometric effect exists. All models must balance bias, underfitting a model to improve generalizability, against variance, overfitting a model to reduce error. A model that captures the effect of composition and the effect of geometry would overfit to this limited data set.

Limiting the scope of the model to a single composition, as in Figure 4(c), exposes the effect of part geometry on the yield strength. While small at 5% of the actual yield strength, a clear variation exists that can be modeled by part spacing, with only a small effect from part location in the plane of the build. As seen in two metrics—the root-mean-square in the standardized errors is 1.72 (an RMS of 1 in the standardized errors is perfect for a gaussian process) and only 54.8%, not 68%, of samples fall within one standard deviation—there is certainly room for improvement in this model. However, the fact that the model underestimates the actual uncertainty, as seen by the wider-than-ideal distribution in Figure 4(d), would suggest that either geometry alone is not a sufficient predictor of yield strength, that is, a large model variance, or that more data is needed to reduce the intrinsic variance. Although we hypothesize that the

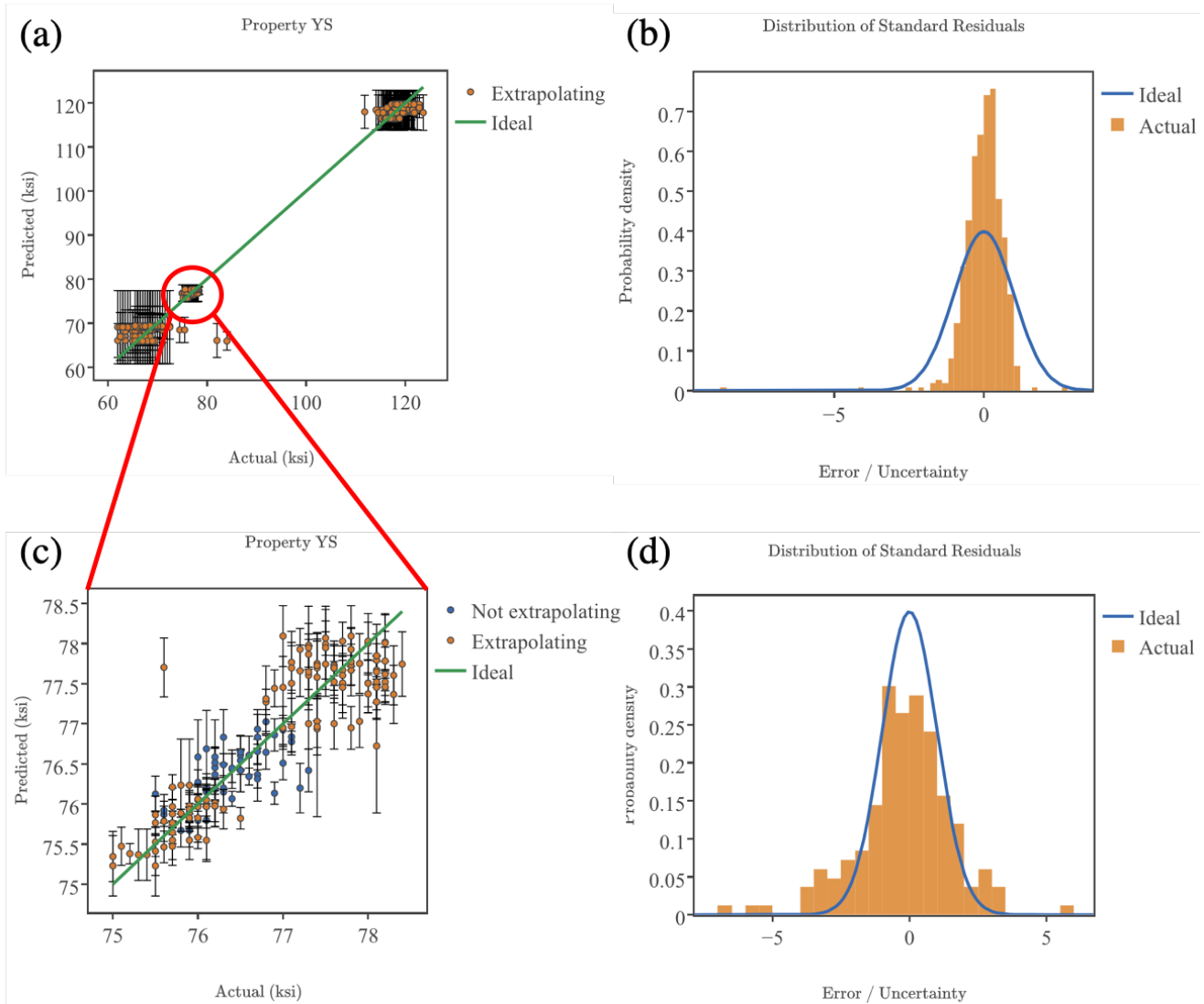


Figure 4. (a) Predicted-versus -actual curve presents a model fit across three compositions, forming three clusters that are, from bottom left to top right, SS 316L, 17-4 PH, and Ti-6Al-4V. (b) The distribution in the model predicted error from (a). (c) The predicted-versus-actual plot in presents the efficacy of the model in capturing the 5-7% variability in 17-4 PH yield strength. (d) The distribution in the model predicted error from (c).

simplicity of a geometry-only model in a process as complex as additive manufacturing suggests the former, the database of printing parameters, including laser speed, spot size, hatch spacing, and laser power, must be modified to increase model complexity sufficiently to capture more of this variability.

Finite Element Analysis

The FE model was used to assist in the optimization of the AM builds of the hinge parts by identifying regions of stress under simulated loading. When applying the specified loads to the door and hinge assembly, the hinge pin exhibited a von Mises stress state that was an order of magnitude larger than any other component in the assembly that was analyzed.

The principal stresses calculated in the pin are presented in Figure 5. A length-wise, cross-sectional view of the pin is shown in Figure 4(a). There are two regions, roughly one third from the top and bottom of the pin, that exhibit the highest stress concentrations. These regions correspond to the interfacing areas of the two hinge plates with the hinge pin.

Figure 5(b),(d),(f) correspond to the axial principal stresses, while Figure 5(c),(e),(g) correspond to the shear principal stresses. As shown, the critical stress state at the highlight portion of the pin contains both shear and tension components. As such, the critical stress state yielded a von Mises stress of 980 MPa.

Furthermore, the calculated critical stress exceeds the minimum strength specification of 890 MPa set for the pin of the legacy hinge assembly. Changes to in-field services conditions are stated to have increased the weight of the door, which has the potential to result in a stress state for the pin beyond its originally engineered specifications.

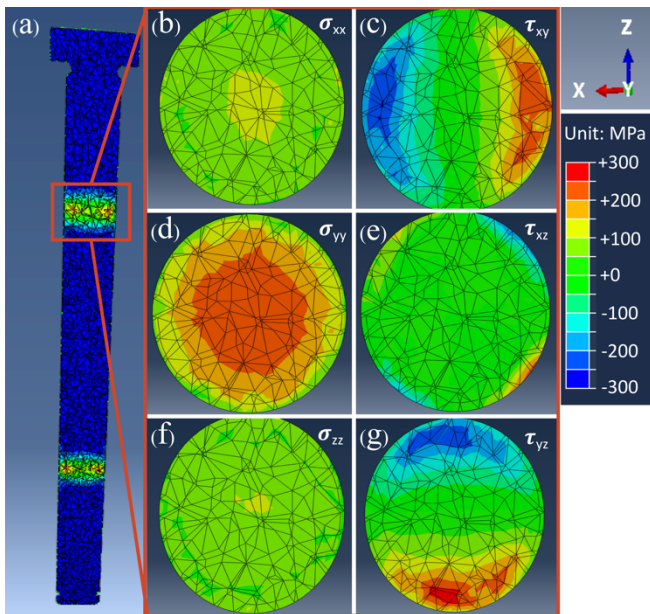


Figure 5. Finite element modeling showing (a) the regions between the interfaces of the hinge plates and the pin as being the highest stress state locations. The axial principal stresses [(b), (d), and (f)] and shear principal stresses [(c), (e), and (g)] indicate a combined tension-shear stress condition.

3.2. Validation of AM Replacement Parts

The direct AM replacement parts are shown in Figure 2. In order to validate these parts, the material properties and performance were evaluated by monotonic tensile, biaxial tension-torsion fatigue, and full-assembly failure tests.

Monotonic Tensile Testing

To evaluate the degree of anisotropy that can be observed in AM materials [3], specimens were sectioned according to Figure 2(c). Specimens for the AM replacement part were evaluated in the as-printed and after heat treatment (CA+H900) conditions.

The monotonic tensile properties for the legacy and AM replacement parts are reported in Table 1. The as-printed condition exhibited limited anisotropy in terms of yield strength (YS), this effect was more pronounced when examining ultimate tensile strength (UTS). The specimen perpendicular to the build direction exhibited at least an 8% increase in UTS over other orientation evaluated. The elastic modulus, save the LG1 sample orientation, was constant regardless of orientation. Additionally, no anisotropy was observed with respect to elongation to failure.

With the application of heat treatment, the effects of precipitation hardening were greatly observed. The CA + H900 specimens exhibited increases of 64% and 70% in YS and UTS, respectively. Moreover, the increases in strength was accompanied by a 57% reduction in elongation to failure. In terms of anisotropic effects, the strengths across all build orientation did not vary by more than 4%, thus the effects were limited.

Comparing the as-printed and legacy conditions, the yield strength was on average 70% higher for the as-printed condition. Yet, the UTS for each condition was within 3% overall, save sample orientation LG3.

Table 1. Monotonic tensile properties of legacy and AM replacement parts.

Sample	Condition	E (GPa)	σ_{YS} (MPa)	σ_{UTS} (MPa)	% Elongation
LG1	Legacy	170 ± 2	402 ± 5	746 ± 2	18.8 ± 1.4
	As-Printed	148 ± 6	741 ± 4	755 ± 13	16.0 ± 0.9
	H900 HT	196 ± 8	1195 ± 20	1279 ± 32	7.4 ± 0.4
LG2	Legacy	175 ± 14	429 ± 1	768 ± 6	18.3 ± 1.4
	As-Printed	162 ± 7	726 ± 14	762 ± 9	17.8 ± 0.9
	H900 HT	185 ± 16	1225 ± 20	1308 ± 22	8.3 ± 0.7
LG3	Legacy	169 ± 13	437 ± 13	765 ± 18	16.7 ± 0.8
	As-Printed	168 ± 6	781 ± 6	820 ± 5	15.7 ± 1.2
	H900 HT	169 ± 15	1235 ± 11	1319 ± 6	8.7 ± 1.4
SM	Legacy	165 ± 12	477 ± 23	767 ± 17	16.5 ± 1.1
	As-Printed	172 ± 21	720 ± 7	751 ± 6	17.3 ± 1.6
	H900 HT	182 ± 13	1237 ± 3	1329 ± 7	4.3 ± 1.6

In terms of the monotonic tensile properties, the AM direct replacement part has shown comparable performance to that of the legacy part. Furthermore, once heat treated to the CA +H900 condition, the material performed to the specified strength conditions of the legacy hinge pin (min. 890 MPa strength requirement). Thus, the strength requirements for the legacy hinge were met and even exceeded by the AM direct replacement part.

Tension-Torsion Fatigue Testing

In an attempt to simulate the combined stress state calculated from FEA as detailed in Section 3.1, biaxial tension-torsion fatigue tests were performed on the hinge pin. The conditions examined were the legacy hinge pin, as-printed pin, and after CA + H900 heat treatment.

The number of cycles to failure for each condition examined is presented in Table 2. The hinge pins in the legacy condition exhibited the longest fatigue life with an average cycle to failure of 507,819. The second-best performing was the as-printed condition, with 89,812 cycles to failure. Lastly, CA + H900 condition failed at an average cycle count of 47,544.

At these intermediate fatigue regimes, there is a transition in failure mechanism from material-based to defect-based. One plausible explanation for the reduced fatigue performance is AM can generate porosity defects through keyholing and lack-of-fusion mechanisms [3]. It is to be expected that the AM parts, to a degree, contain such defects, especially at the surface of the fatigue specimens. As such, these defects would serve as stress concentrators that would reduce the fatigue life over the legacy counterpart.

Table 2. Average number of cycles to failure for tension-torsion fatigue testing.

Condition	Average Cycles to Failure
Legacy	507,819
As-printed	89,812
CA+H900	47,544

However, in spite of the AM parts achieving ~5X fewer cycles before failure—regardless of AM material condition—given the simulated service length, the AM replacement parts would meet the necessary service requirements to repair and

redeploy the vehicle while the legacy replacement part could be procured.

Additionally, investigation of the material behavior and corresponding macroscopic responses will be the focus of future study.

Full Hinge Assembly Failure

In an attempt to simulate real-life service conditions, full hinge assemblies were destructively tested under three-point bend conditions. The corresponding force-displacement curves for all examined conditions are reported in Figure 6. The full legacy hinge assembly (both hinges plates and pin) (Figure 6(a)) and the legacy hinge plates with as-printed AM replacement pin (Figure 6(b)) exhibit similar force-displacement responses with the knee of the curve around 45 kN. Furthermore, the CA+H900 condition pins (Figure 6(c-d)) showed much higher loads at the knee point in the curves, occurring around 70 kN. Comparing the loads, this roughly equates to a 55% increase in applied load over the legacy part before the onset of the knee point.

Based upon the reported observations, it is suggested that the direct replacement of the failed legacy hinge with an as-printed AM pin may give comparable load responses, which is important in validating the AM replacement parts as a viable option. Through the application of CA+H900 heat treatment, the response for the AM material resulted in higher sustained loads. The implications of increased material performance allow for meeting new in-field service requirements as the result of any vehicle modifications, in addition to allowing for redesign of the legacy part to achieve light-weighting efforts while maintaining structural integrity. Such unique opportunities made possible through AM are hereafter described.

3.3. Opportunities for Resigned Parts using Additive Manufacturing

AM not only offers unique advantages for the procurement process of replacement parts in theater but also gives rise to the ability to modify existing parts for new service requirements, as vehicles are commonly modified from their initial

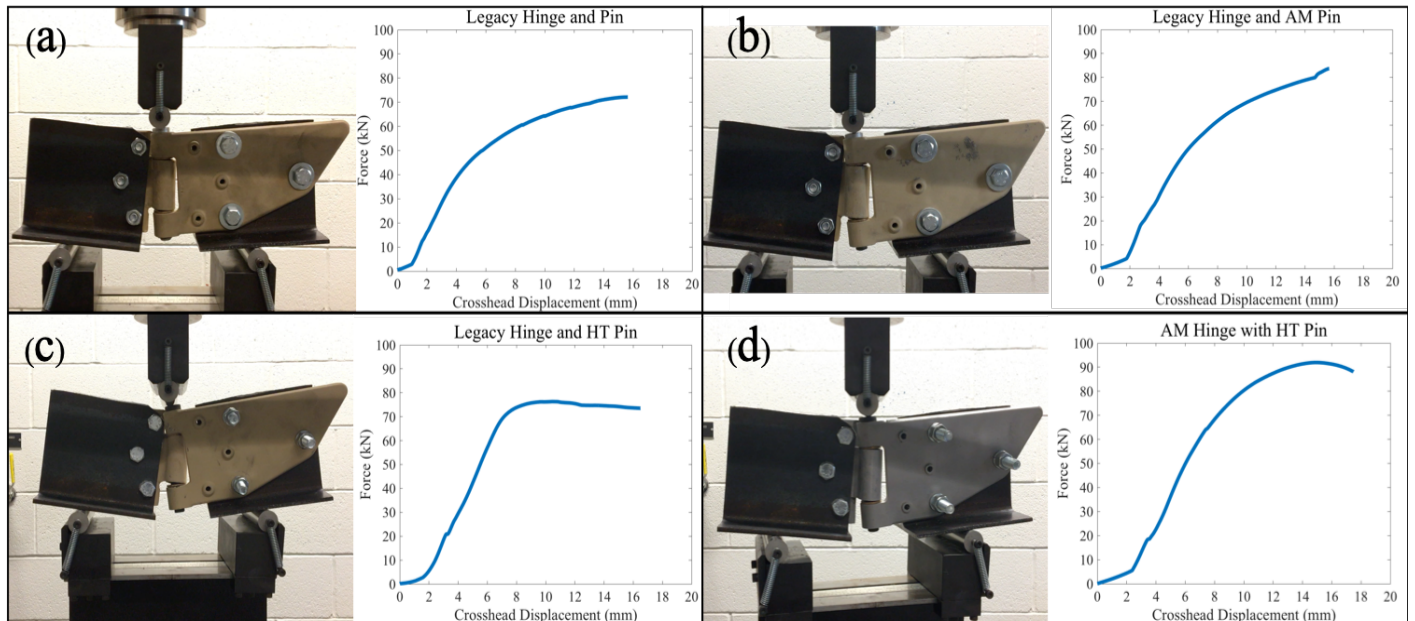


Figure 6. Full hinge assembly failure by three-point bend testing. Force-displacement responses presented for (a) legacy hinge assembly, (b) legacy hinge plates with as-printed AM pin, (c) legacy hinge plates with CA+H900 AM pin, and (d) as-printed AM hinge plates with CA+H900 AM pin.

manufactured condition. Presented in Figure 7 is the first iteration of a “designed for AM” replicate of the legacy hinge assembly. There are several modifications made to the legacy part geometry that allow for the potential of improved part performance. Yet, it is important to note that despite changes to the geometry, the fixturing pattern was maintained to allow seamless implementation on the vehicle without the need for modification.

As shown in Figure 7, regions of the part had reduced thickness or were removed altogether. The new geometry allowed for the part to be printed more easily, as those regions served to alleviate residual stresses that can arise during manufacturing [8]. Furthermore, these reduced and removed regions offer the ability to implement weight savings for existing parts, as vehicle weight is an important consideration with respect to combat effectiveness [9].

Moreover, the part redesign allowed for enhanced performance through enhancing its load capabilities. As identified through FEA and full assembly failure tests, the hinge pin exhibits the highest stress state and is the source of failure for the assembly. With the opportunities afforded by AM, the hinge assembly was redesigned to print as one contiguous piece, eliminating the hinge pin altogether. The new interface consists of a

hemispherical, “ball and socket” connection, as shown in the inset image “Section C-C” of Figure 7. By modifying the design to this interface type, the effective stress state reduced to ~40 MPa, as determined by FEA calculations. This is a reduction of nearly 20x to the existing stress state in the legacy part.

Additional topology optimization would allow for further weight reduction based around the enhanced load performance of this redesigned interface.

4. Conclusions

A statistical framework for the validation and performance quantification using ICME and limited sample testing has been presented.

Coupled with data informatics and modeling, preexisting materials databases were used to construct an accurate process-property mapping for 17-4 PH stainless steel. From this, AM replacement parts were successfully manufactured, and were shown to comparable or enhance performance over the legacy part for monotonic tensile properties and full hinge assembly failure testing. And although the fatigue performance was reduced compared to the legacy part, the duration in which the AM replacement would perform is adequate to allow for sourcing of the legacy part to occur.

Lastly, AM offers immense opportunities in point-of-need part sourcing and the ability to “design for additive,” which is shown to offer enhance performance and weight savings.

In summary, this project demonstrated a framework for continuous improvement in designing and quantifying the performances of AM replacement parts as a means to accelerate their qualification.

5. Acknowledgments

The authors gratefully acknowledge funding from U.S. Army CCDC Ground Vehicle Systems Center.

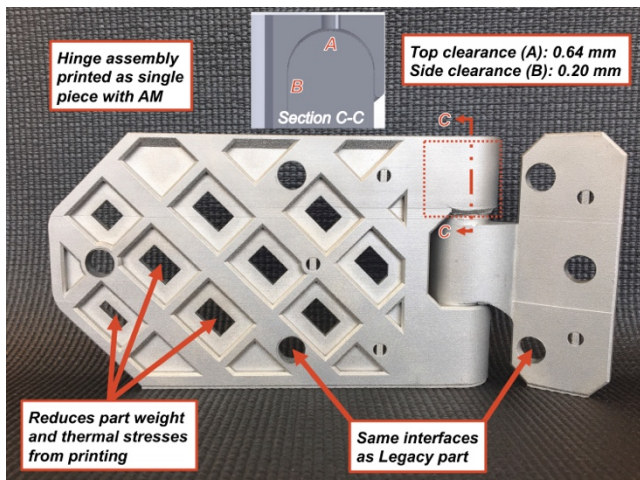


Figure 7. “Design for additive” AM replacement hinge assembly.

REFERENCES

- [1] E. N. Loreda, J. F. Raffensperger, and N. Y. Moore, "Measuring and Managing Army Supply Chain Risk," Report no. RR-902-A, Rand Corporation, Santa Monica, CA, 2015.
- [2] M. Pepi, "Towards Production of Additive Manufacturing Grade Metallic Powders on the Battlefield," Report no. ARL-RP-0618, Aberdeen Proving Ground, MD, Army Research Laboratory, 2017.
- [3] T. DebRoy *et al.*, "Additive manufacturing of metallic components – Process, structure and properties," *Prog. Mater. Sci.*, vol. 92, pp. 112–224, 2018.
- [4] W. E. Frazier, "Metal additive manufacturing: A review," *J. Mater. Eng. Perform.*, vol. 23, no. 6, pp. 1917–1928, 2014.
- [5] M. Seifi *et al.*, "Progress Towards Metal Additive Manufacturing Standardization to Support Qualification and Certification," *Jom*, vol. 69, no. 3, pp. 439–455, 2017.
- [6] L. Breiman, "Random Forests," *Mach. Learn.*, vol. 45, no. 1, pp. 5–32, 2001.
- [7] S. Wager, T. Hastie, and B. Efron, "Confidence Intervals for Random Forests: The Jackknife and the Infinitesimal Jackknife," *J. Mach. Learn. Res.*, vol. 15, no. 1, pp. 1625–1651, 2014.
- [8] F. Bayerlein, F. Bodensteiner, C. Zeller, M. Hofmann, and M. F. Zaeh, "Transient Development of Residual Stresses in Laser Beam Melting - A Neutron Diffraction Study," *Addit. Manuf.*, vol. 24, pp. 587–594, Dec. 2018.
- [9] R. J. Hart and R. J. Gerth, "The Influence of Ground Combat Vehicle Weight on Automotive Performance, Terrain Traversability, Combat Effectiveness, and Operational Energy," In *Proceedings GVSETS 2018*.